JOURNAL OF AIRCRAFT
Vol. 34, No. 3, May–June 1997

Computation of Noise Radiation from Fan Inlet and Aft Ducts

M. Nallasamy*
NYMA, Inc., Brook Park, Ohio 44142

This paper examines turbofan noise radiation characteristics of both the inlet and the aft exhaust ducts using solutions obtained from a finite element code. The far-field principal lobe peak angle variations with mode cutoff ratio, duct Mach number, and external flow Mach number are examined. The predicted far-field principal lobe peak angle variations compare very well with the available analytical results. It is found that the principal lobe peak angle of the inlet radiation is insensitive to the duct and external flow Mach numbers. In the case of the aft duct, an increase in duct Mach number moves the principal lobe away from the aft duct axis, whereas an increase in external flow Mach number moves the principal lobe toward the aft axis. The solutions (for both inlet and exhaust duct radiation) also show that the far-field radiation principal lobe peak angle is only a function of cutoff ratio and nearly independent of the mode number. The ability of the code to handle ducts with acoustic treatments is also demonstrated.

Introduction

ONE of the major sources of noise in aircraft turbofan engines is the fan noise. The noise radiated from the fan inlet and aft ducts is of great concern during takeoff and landing. It is recognized that the fan noise is a critical component controlling the total noise at takeoff and approach conditions.[1] Stringent limits on airport noise levels and curfews necessitate a better understanding of the noise generation mechanisms and the noise suppression techniques to alleviate community noise problems.

A typical fan noise spectrum consists of tone noise [blade passing frequency (BPF) and its harmonics] superimposed over broadband noise. The tone noise component is the result of the interaction of the periodic disturbances of the rotor blade mean (viscous) wake with stator vanes. This is usually referred to as rotor–stator interaction noise and is the component considered here. The acoustic pressure distribution in the duct can be expressed in terms of normal modes once the pressure dipole distribution on the blades is known. The blade pressure distribution is usually computed using quasi-three-dimensional techniques or strip theory that employs local two-dimensional approximations.

The generated noise may consist of propagating and nonpropagating or decaying modes. The propagating modes travel to the duct exit and propagate to the far field. The noise radiation to the far field may be computed using analytical methods or finite volume/finite element numerical techniques. The finite volume/finite element techniques have the advantage of modeling the geometry accurately. The finite element technique and computer codes developed[2,3] and applied to modern turbofans[4,5] are used in the present study. This study forms part of an effort to benchmark the validity of the finite element solutions obtained using the code mentioned earlier. The benchmarking, however, is done here only by comparing with the available analytical results. Some comparisons of the solutions of the finite element code with the experimental data are reported in Refs. 6 and 7.

Presented as Paper 96-1769 at the AIAA/CEAS 2nd Aeroacoustics Conference, State College, PA, May 6–8, 1996; received May 27, 1996; revision received March 7, 1997; accepted for publication March 9, 1997.

*Senior Engineering Specialist, Aeromechanics Department. Senior Member AIAA.

In this paper, attention is focused on the radiation of noise to the far field from the inlet and aft ducts of the fan. The results of a parametric study of the inlet/aft radiation are presented. Several characteristics of the fan noise radiation pattern are examined through finite element solutions. The results of the finite element solutions are compared with the available analytical results. The capability of the solution technique to handle ducts lined with sound-absorbing materials is also examined.

Duct Acoustics

The idea of analyzing the fan noise in terms of the spinning pressure patterns in the fan duct was first introduced by Tyler and Sofrin.[8] They resolved the sound field into annular duct modes, with spinning order m (number of wavelengths in the circumferential direction) and radial order n (number of nodes or zero crossings of pressure in the radial direction). The radial distribution of pressure in an annular duct is expressed in the form

$$p(r) = c_{mn}[J_m(k_{mn}r) + Q_{mn}Y_m(k_{mn}r)] \tag{1}$$

J_m and Y_m are the Bessel functions of the first and second kind, respectively; k_{mn} is the eigenvalue of the radial wave number for the (m, n) mode; and k_{mn} and Q_{mn} are functions of hub–tip ratio. c_{mn} is the modal amplitude, and r is the radius normalized by the duct radius r_0. The mode shape is independent of the duct flow Mach number.

A spinning mode of order m and frequency ω will propagate through the duct only if its cutoff ratio is greater than or equal to unity. The cutoff ratio is defined as

$$\xi = \frac{(\omega/c)r_0}{k_{mn}\sqrt{(1 - M_d^2)}} \tag{2}$$

where M_d is duct Mach number, ω is frequency in rad/s, k_{mn} is mode eigenvalue, c is the speed of sound in m(ft)/s, and r_0 is the duct radius in m(ft). If the cutoff ratio is less than unity, the mode decays or is cut off. If the rotor in a fan stage contains B rotor blades and the stator contains V vanes, the interaction will set up circumferential mode order m given by $m = sB \pm kV$. s is the harmonic of the BPF tone and k is an integer. The speed of rotation of mode m is (sB/m) times rotor speed. By choosing the correct number of blades and vanes, the BPF

and one or more of its harmonics may be cutoff, reducing the noise generated.

Inlet Radiation

Eversman and Danda Roy[2] solve the radiation problem by a finite element method. The turbofan inlet is assumed to be axisymmetric, and the computational domain is reduced to a two-dimensional meridional plane. The propagation in the duct and the radiation to the far field are included in one model. The inlet flow is assumed to be irrotational. The acoustic problem is formulated in terms of the acoustic perturbation velocity potential. They solve the duct eigenvalue problem for the duct with uniform flow. The duct eigenvalue problem is described by a Bessel's equation of order m. The finite element solution of this equation is the approximation to the exact solution given by Eq. (1). They employ a Galerkin-type finite element formulation with isoparametric elements. The mean flow is computed using a velocity potential formulation, on the same mesh as that used for acoustic propagation and radiation. The acoustic field equations are written in terms of the acoustic potential and acoustic pressure and solved using finite element techniques.

The sound source at the source plane (fan face) is modeled in terms of modal amplitudes [Eq. (1)]. The acoustic potential field is modeled in terms of incident (positive) and reflected (negative) uniform duct eigenfunctions that are matched to the finite element solution on the source plane.[2] When the input to the acoustic radiation problem is given in terms of specified value of incident modal amplitude (as in the present study), the reflected mode amplitude is obtained as a part of the solution. The near-field region is modeled using conventional isoparametric finite elements. Wave envelope elements are used in the far field, assuming that the sound field there approximates that produced by a point source. It is assumed that only outgoing waves exist at the far-field boundary. A Sommerfeld radiation condition for a monopole in a uniform flow is applied there. The same boundary conditions are applied at the baffle boundary. With the wave envelope elements in the far field, the entire radiation field can be modeled with a relatively small number of finite elements. The solution to the finite element system is obtained using a frontal solution method. Further details of the finite element formulation and the solution procedure may be found in Ref. 2.

Aft Radiation

The equations governing the acoustic field of the aft radiation are the same as that of the inlet. However, the jet shear layer introduces complications for the computation of the mean flow. The shear layer is modeled as though the duct is extended several duct radii beyond the exit plane. Along the streamline representing the shear layer a connectivity for potential flow is constructed (in the finite element mesh generation), which allows for a discontinuity in velocity potential. Beyond the extended duct region the velocity potential is continuous. The steady mean flow treated as a duct flow is allowed to mix on a potential flow basis with the external flow, beyond the extended region. The extent of the extended duct region can be varied. It is chosen to provide sufficient distance for full effect on acoustic radiation and long enough to move the rather artificial mixing region away from the important part of the acoustic field.[3] This kind of treatment of the shear layer is found to work reasonably well for the low Mach number flows considered in this paper.

The presence of the shear layer separating the duct flow and external flow necessitates the specification of two continuity conditions for acoustic perturbations along the interface. One is the continuity of acoustic pressure across the shear layer. The second is the kinematic condition arising from the assumption that the interface, between the duct flow and external flow, acts as an impermeable membrane across which acoustic perturbations are transmitted by the motion of the membrane. The displacement of the membrane is the same viewed from the duct flow side or external flow side of the membrane.[3] Other boundary conditions are treated the same way as in the inlet radiation code. Further details of the aft radiation problem and the solution method may be found in Ref. 3.

Duct Lining

One of the fan noise suppression techniques is to line the duct walls with materials of appropriate surface impedance to absorb part of the generated fan noise. The finite element technique developed by Eversman and Danda Roy[2] can handle lined surfaces by specification of the impedance of the treated elements. The impedance z is equal to $p/v\cdot n$, where p is the acoustic pressure and $v\cdot n$ is the normal component of the velocity at the lined wall; z is normalized with respect to $(\rho c)_\infty$. The lined element is defined in terms of its normalized impedance

$$z = R + iX \tag{3}$$

where R is the normalized resistance and X is the normalized reactance.

Fan Geometry

The present computational study was done using the geometry of the active noise control (ANC) fan that is being tested in the Aeroacoustic Propulsion Laboratory at NASA Lewis Research Center.[6,7] A top-view schematic of the NASA ANC fan rig[6] is shown in Fig. 1. The 4-ft-diam fan has a max-

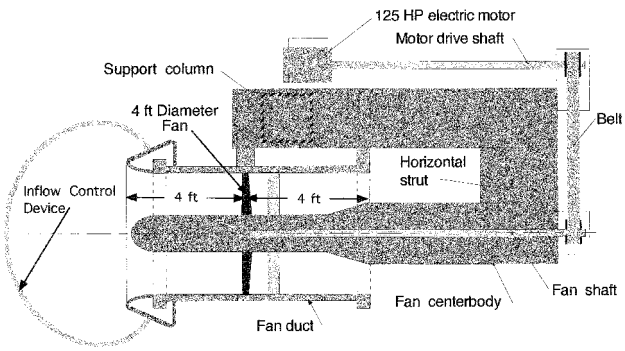

Fig. 1 Top view schematic of NASA ANC fan rig.

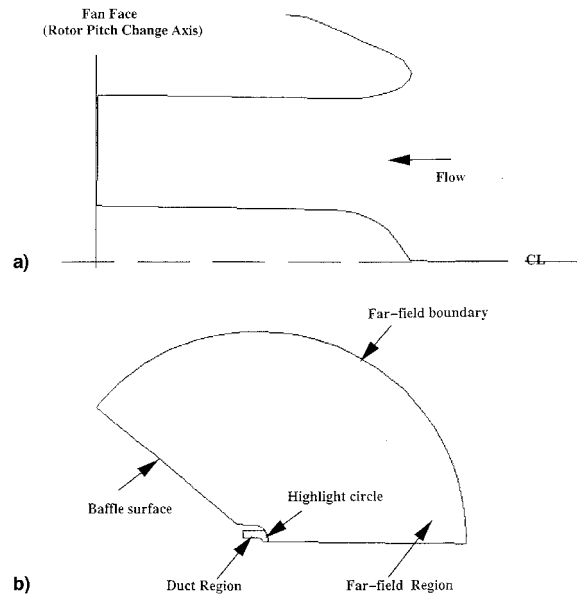

Fig. 2 a) Inlet geometry sketch and b) computational domain.

imum tip Mach number of 0.35 at the design speed of 1886 rpm. The fan hub-to-tip ratio is 0.307 and the average blade chord is 4.5 in. The duct has a constant diameter over the entire length. Nozzle area contraction is accomplished by an increase in the centerbody diameter to where the exit plane hub-to-tip ratio is 0.5. A long centerbody and a flanged exit characterizes the aft duct. Further details of the fan may be found in Ref. 6.

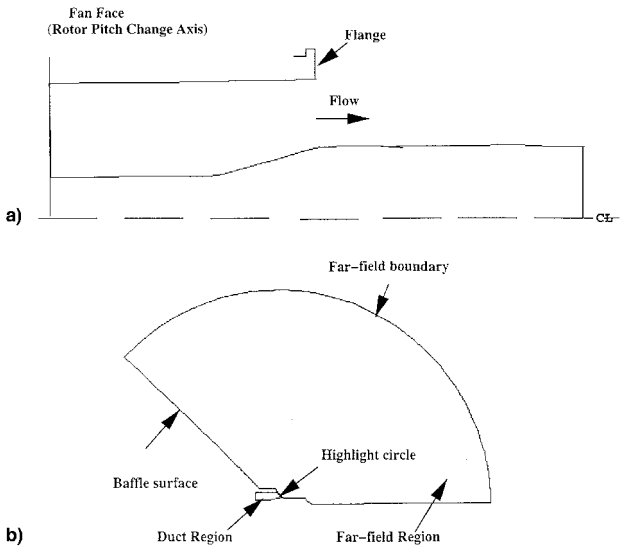

Fig. 3 a) Aft geometry sketch and b) computational domain.

For the purpose of this study the source (input) plane is chosen as the rotor pitch change axis (fan face), and a unit mode amplitude is used as the input for each mode. The propagation through the inlet and aft ducts and the respective far-field radiation are studied. The computation is carried out separately for the inlet and aft radiation. The inlet geometry and computational domain are shown in Fig. 2. The aft duct geometry and computational domain are shown in Fig. 3. The far-field boundary and baffle boundary are shown in both figures. The far-field boundary is located at 20 duct radii where far-field measurements are made.

The rotor has 16 blades and the number of vanes has been varied in tests to study different aspects of the radiation characteristics. However, for the present study, a 14-vane stator is used, resulting in the following propagating modes at the design speed: BPF: (2,0), 2BPF: (4,0), (4,1), 3BPF: (6,0), (6,1), (6,2), (−8,0), and (−8,1). The propagation characteristics of these modes in the inlet and exhaust ducts and their radiation to the far field are examined using the finite element method described earlier. The fan radius is 2 ft and the design speed is 1886 rpm. The fan face Mach number is 0.1 and there is no external flow.

Results and Discussion

Far-Field Directivities

The results of the parametric computational study of the inlet and aft radiation patterns of the ANC fan are presented and discussed. The input modal amplitude of each mode is specified as unity in the study to obtain the general picture of the radiation patterns. At any circumferential mode order m,

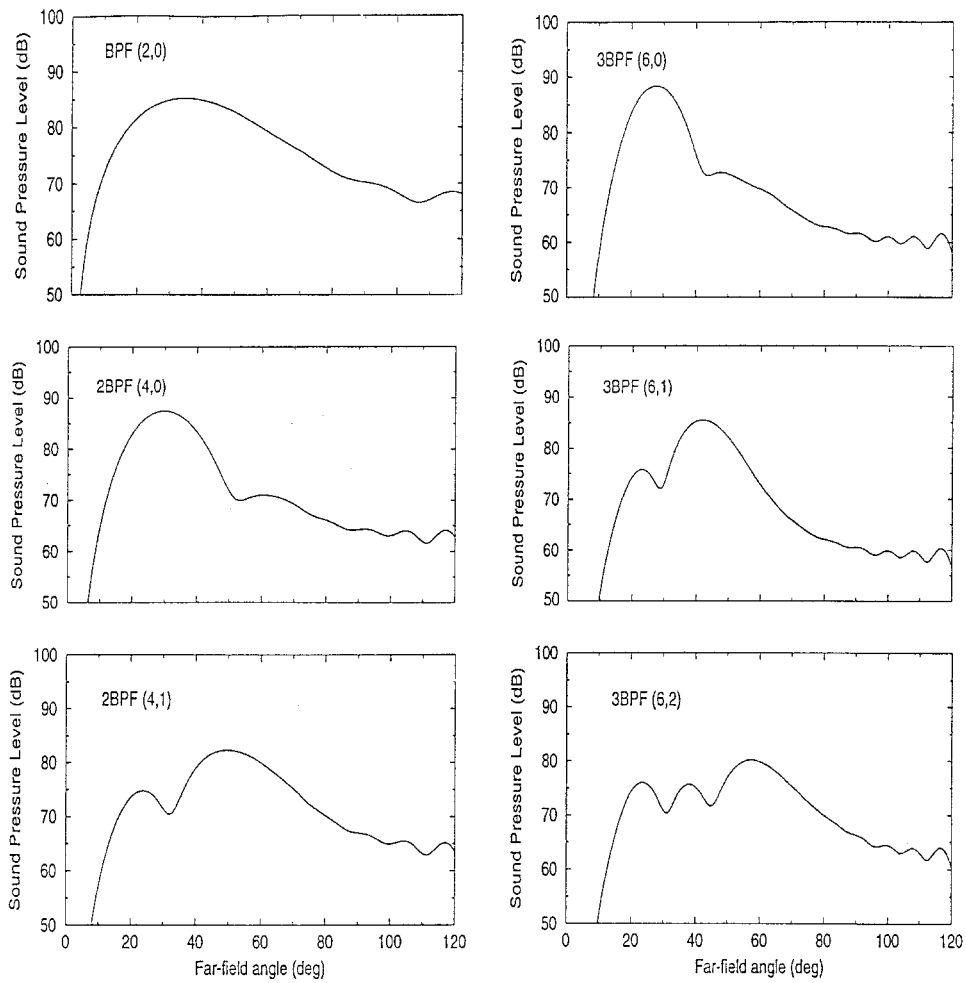

Fig. 4 Far-field directivities: inlet radiation, 16 blades, 14 vanes, 1886 rpm.

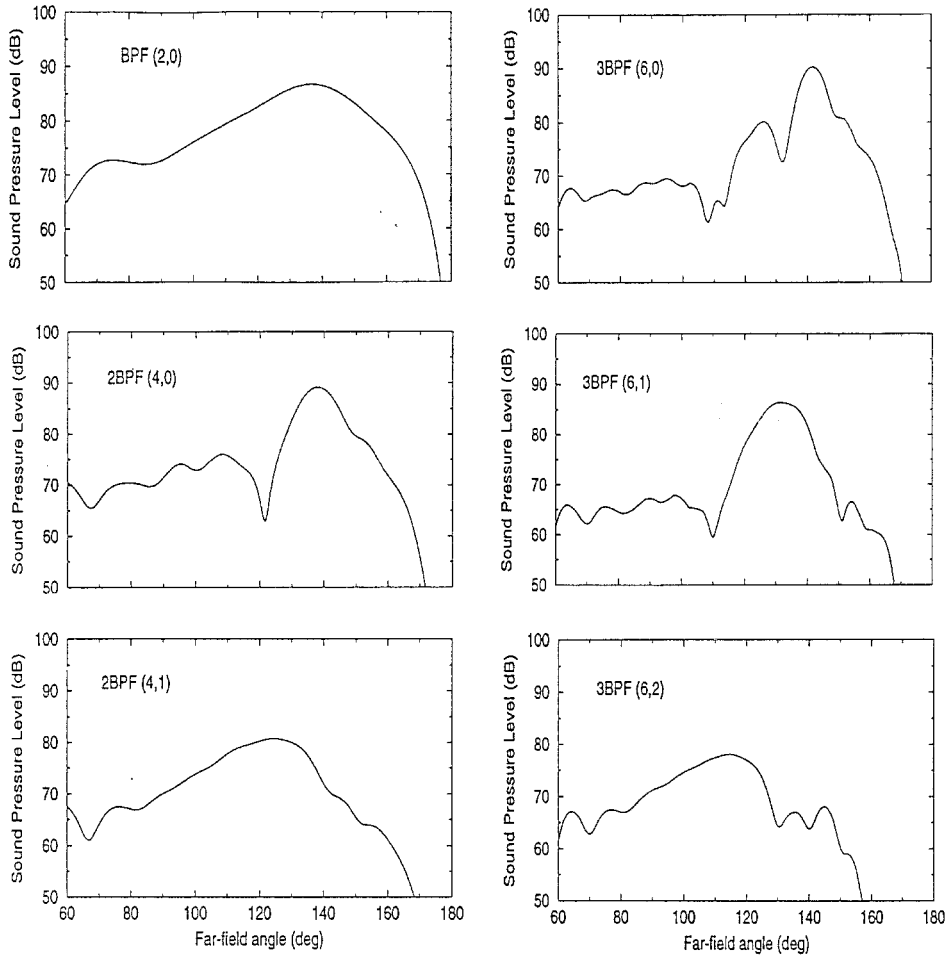

Fig. 5 Far-field directivities: aft radiation, 16 blades, 14 vanes, 1886 rpm.

the radial order mode shapes are given by the Bessel functions (of the first and second kind) as described in Eq. (1). The far-field directivities of noise radiated from the inlet duct for modes (2,0), (4,0), (4,1), (6,0), (6,1), and (6,2) are shown in Fig. 4. The far-field angle is measured with respect to the inlet axis. The principal lobe size decreases with increases in harmonic order for the zero-order radial mode. When there are higher radial order propagating modes, as in 2BPF and 3BPF, the zero-order mode has higher sound pressure level (SPL). Note that the input model amplitude of the modes is held constant (unity). Successively higher radial-order modes show reduction in SPL and the principal lobe angle moves away from the axis. For the radial order $n = 1$, one side lobe develops, while for $n = 2$ two side lobes appear. Far-field shape measurements by Cumptsy[9] show similar behavior of different radial orders at low speed. Thus, the qualitative features of the computed far-field shapes are consistent with the experimental observations. The small oscillations in SPL beyond 90 deg are because of the spurious reflections from the baffle boundary, but are well below the peak SPL.

The far-field directivities of the aft duct radiation for modes in BPF, 2BPF, and 3BPF are shown in Fig. 5. It is seen that modes (4,0) and (6,0) develop side lobes (away from the aft axis), the one for (6,0) being more pronounced. This appears to stem from the exit flange and is absent in the inlet directivities (Fig. 4). However, the side lobes equal to the number of the radial order appearing near the axis observed at the inlet appear also in the aft far-field directivities, but are far less pronounced. The far-field shapes for different radial orders show behaviors similar to those observed for the inlet radiation.

A composite picture of the far-field directivity from 0 to 180 deg, combining the inlet and aft radiation results, is shown in Fig. 6a for the BPF. (Recall that an equal mode amplitude is input at the source plane for inlet and aft propagating modes). In the intermediate region where the radiation from the inlet and aft interfere with each other, the mean square pressures from the inlet and aft have been added to get the resultant curve. It is thus possible to compute the entire far-field directivity using the present inlet and aft radiation codes. Such computations have been made and compared with ANC test data and reported elsewhere.[6,7] The acoustic pressure contours in the inlet and aft ducts and in their far-field regions are shown in Fig. 6b. The pressure contours in the inlet duct show the expected radial variation for the (2,0) mode. The aft duct with changing cross-sectional area, flanged duct, and long centerbody influence the pressure distribution near the exit plane. The maximum pressure occurs in the duct rather than near the wall for the (2,0) mode. The ANC test data also show a similar profile with off-the-wall maximum for this mode.

Far-Field Principal Lobe Angle

Rice et al.[10] studied the relation between the propagation angle in the duct and the far-field radiation. The angle made by the normal to the local wave front with the coordinate axes is defined as the mode propagation angle. They found that the mode propagation angle in the duct closely approximates the angle of the principal lobe of the far-field radiation. The far-field lobe angle in the referenced study was obtained using the Wiener–Hopf technique. The expression for the principal lobe angle for no flow is given by

$$\cos \psi_p = \sqrt{1 - 1/\xi^2} \tag{4}$$

ξ is the cutoff ratio of the (m, n) mode.

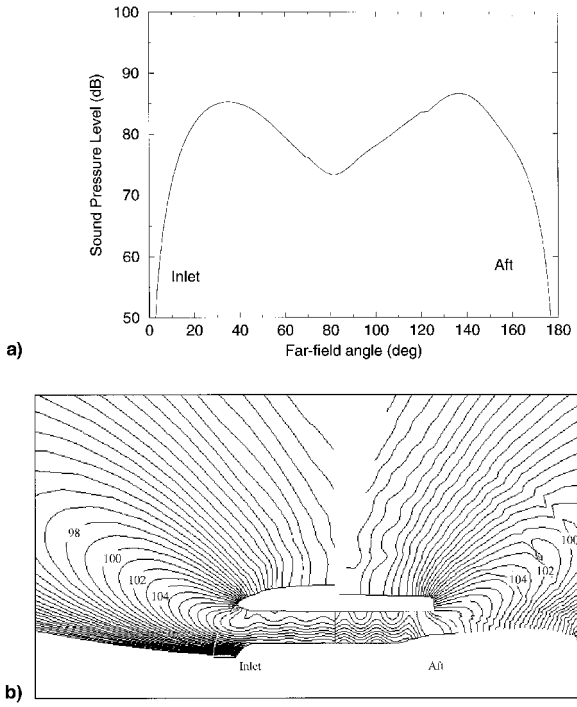

Fig. 6 a) Far-field BPF directivity: inlet and aft radiation, 16 blades, 14 vanes, 1886 rpm. b) Acoustic pressure contours (dB): BPF, contour interval = 1 dB, maximum = 120 dB, minimum = 80 dB.

When the duct Mach number is zero, the equation for the principal lobe angle applies to the aft duct as well.

The radiation directivity patterns of acoustic modes in an unflanged circular duct with and without uniform flow in the duct was presented by Homicz and Lordi.[11] The expression for the principal lobe angle when there is uniform flow in the duct is given by Homicz and Lordi[11] as

$$\cos \psi_p = \beta \sqrt{\frac{(1 - \zeta^2)}{[1 - M_d^2(1 - \zeta^2)]}} \tag{5}$$

where

$$\zeta = \frac{k_{nm}}{[(\omega/c)r_0/\beta]}$$

$$\beta = \sqrt{(1 - M_d^2)}$$

Radiation from the aft duct of a turbofan was analyzed by Savkar,[12] allowing for the velocity and temperature mismatch between the external and duct flows. Rice and Saule[13] developed an approximate method for aft duct radiation. It has been found that their far-field radiation results[13] are in good agreement with that of Savkar.[12] The principal lobe angle for the aft duct radiation is given by Rice and Saule[13] as

$$\cos \psi_p = \frac{-M_d + \xi\sqrt{\xi^2 - 1}(1 - M_d^2)}{\xi(1 - M_d^2)(\xi + M_d\sqrt{\xi^2 - 1})} \tag{6}$$

for the case of no external flow.

Effect of Cutoff Ratio

For the case of no external flow (static), Eversman's radiation code[3] was run for mode (4,0) at different cutoff ratios for a duct Mach number of zero and the far-field principal lobe angles obtained for the inlet and aft radiation are shown in Fig. 7. Also shown on the plot are the values of the lobe angle

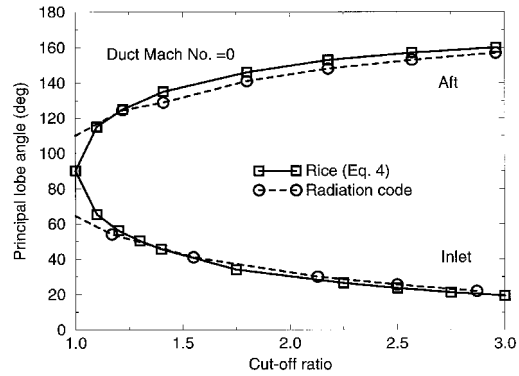

Fig. 7 Principal lobe angle variation with cutoff ratio. External flow Mach number = 0, mode = (4,0).

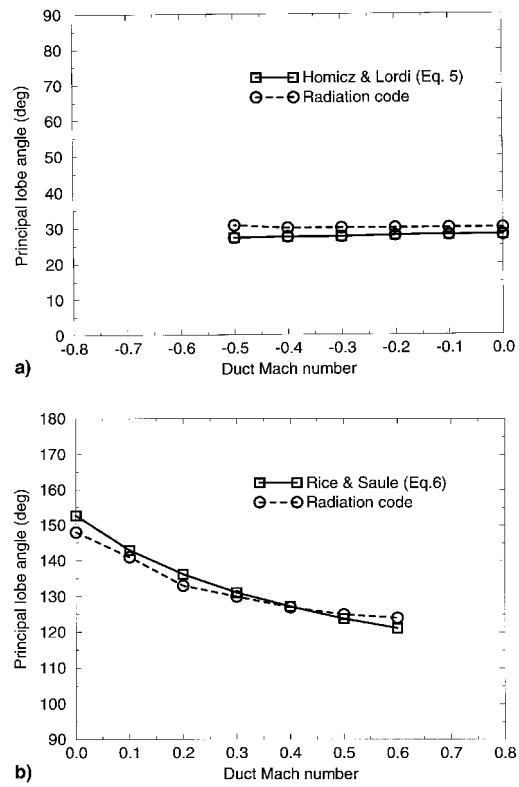

Fig. 8 Principal lobe angle variation with duct Mach number. External Mach number = 0, mode = (4,0): a) inlet and b) aft.

given by Eq. (4). It is seen that for cutoff ratios less than 1.2, the principal lobe angles predicted by Eversman's code[3] differ from that of Eq. (4). This is partly because of the baffle boundary location (Figs. 2 and 3) and the boundary condition employed in the computations. Near cutoff, the radiation is toward the sideline and that is when the influence of the baffle boundary and the far-field radiation condition imposed on it creeps into the solution.

Duct Flow Effects

The variation of the far-field principal lobe angle with duct Mach number is shown in Fig. 8. An increase in the duct Mach number moves the lobe angle of the inlet radiation very slightly toward the inlet axis according to Eq. (5). Finite element solutions based on Eversman's code also indicate that the far-field lobe angle is nearly insensitive to the duct flow Mach number. For the aft duct, the far-field lobe angle variation with duct Mach number along with the curve given by Eq. (6) is shown in Fig. 8b. The agreement between the Eversman computations[3] and Eq. (6) is good. It should be noted

that Eqs. (4), (5), and (6) are analytical approximations derived for circular ducts (no centerbody).

External Flow Effects

Figure 9 shows the variation of principal lobe angle with external flow Mach number for three different duct Mach numbers. For the inlet where the sound propagation is opposite to the direction of the flow, the principal lobe angle is insensitive to the external Mach number for the three duct Mach numbers considered. For the aft duct, however, an increase in external flow Mach number causes the principal lobe to move toward the exit duct axis. This increase in principal lobe angle is more pronounced for the lower duct Mach number of 0.2. This is consistent with the results of Savkar.[12]

Cutoff Ratio and Far-Field Principal Lobe Peak Angle

Rice[14] studied the far-field radiation pattern for single and multimodes as a function of cutoff ratio. An important contribution is the finding that all modes with approximately the same cutoff ratio will have approximately the same angle for the principal lobe peak of the far-field radiation pattern. This concept is examined with the inlet and aft radiation codes by obtaining far-field radiation patterns for different mode orders at a cutoff ratio of 1.5. Figure 10 shows the far-field lobe pattern for the inlet and aft duct radiation for modes (2,0), (4,1), (6,2), and (−8,0). The principal lobe angle for the inlet radiation for all the modes is about 43 deg (Fig. 10a). It is seen that the far-field lobe angle for the aft duct for all of the modes is approximately 130 deg (Fig. 10b). The theoretical principal lobe peak angles [Eqs. (5) and (6)] for the present case are 42 deg for the inlet and 131 deg for the aft. Thus, the inlet and aft radiation codes are able to predict far-field peak radiation angles consistent with the theory.

Effect of Liner

The Eversman radiation codes[3] can handle the lined ducts by specifying the surface impedance of the lined elements in the finite element system. To demonstrate this capability, the code was run with specified wall impedance for the lined region of the duct. It should be noted that the results presented here are for demonstration purposes only and no test is run on the ANC fan with acoustic lining. The inlet lining impedance was chosen to be close to the optimum impedance at BPF, obtained by extrapolation from the optimum impedance curves of Rice,[15] based on mode cutoff ratio. For simplicity, the same impedance was used for both the inlet and aft ducts. The location of the lined sections of the ducts are shown in Fig. 11. In actual turbofan engine applications, the acoustically lined section is usually located in the straight portion of the duct and the lining is also used on the centerbody. The code handles lined elements on the nacelle as well as the centerbody. In the present computations, the lining in both ducts is only on the nacelle surface, as shown in the figure, and starts $0.061r_0$ from the exit plane. The length of the lined region is $0.55r_0$ in the inlet duct and $0.53r_0$ in the aft duct. The impedance chosen is

$$z = 0.45 - i0.40$$

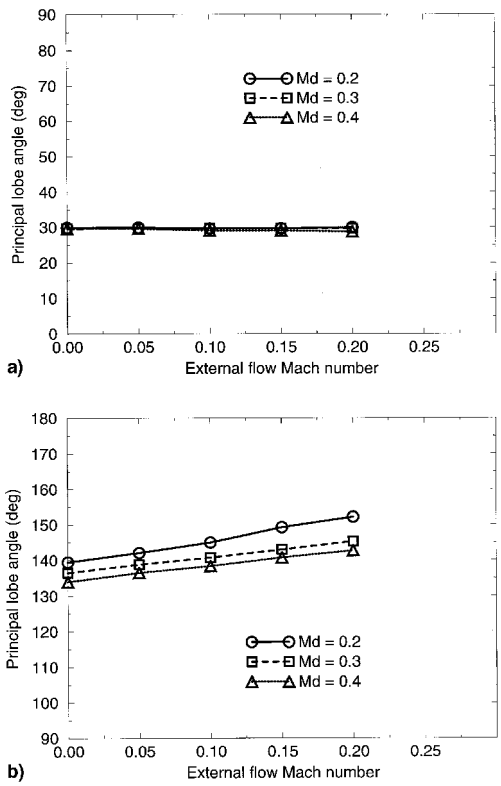

Fig. 9 Principal lobe angle variation with external Mach number. Mode = (4,0): a) inlet and b) aft.

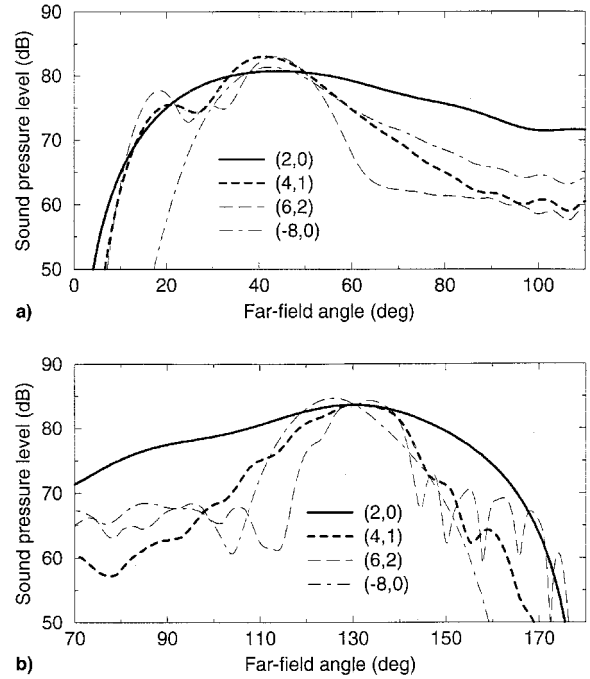

Fig. 10 Far-field shapes of four different modes at a cutoff ratio of 1.5: a) inlet and b) aft.

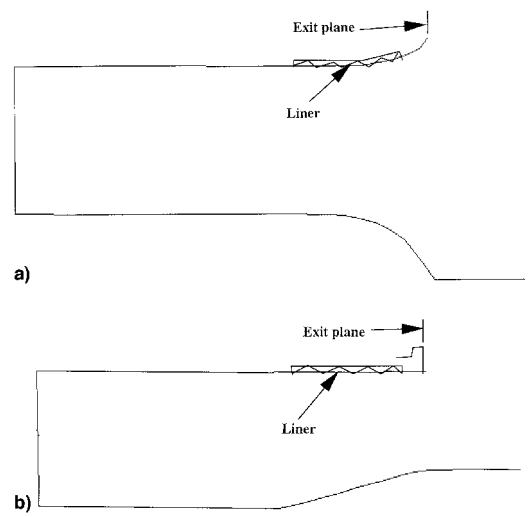

Fig. 11 Liner locations: a) inlet duct and b) aft duct.

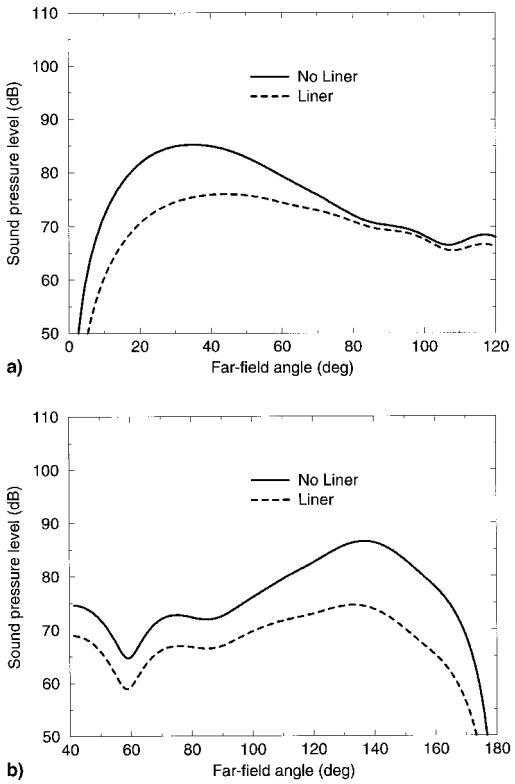

Fig. 12 Far-field shapes. Effect of liner, $z = 0.45 - i0.40$: a) inlet and b) aft.

The far-field acoustic pressure directivities for mode (2,0) at the inlet and at the aft are shown in Fig. 12. It is seen that in either case the noise attenuation caused by the liner is not uniform at all of the angles.

Concluding Remarks

Turbofan inlet and aft noise radiation characteristics were examined for a low-speed fan using a finite element code. It is shown that the inlet and aft radiation characteristics predicted by the finite element codes are in fair agreement with theoretical calculations. The effects of cutoff ratio, duct Mach number, and external flow Mach number variations on the far-field principal lobe peak angle were presented. The capability of the codes to handle ducts with acoustic lining was demonstrated.

Acknowledgments

This work is sponsored by NASA Lewis Research Center under Contract NAS3-27186 with John F. Groeneweg and Dennis L. Huff as Project Managers.

References

[1]Groeneweg, J. F., and Rice, E. J., "Aircraft Turbofan Noise," *Journal of Turbomachinery*, Vol. 109, No. 1, 1987, pp. 130–141.

[2]Eversman, W., and Danda Roy, I., "Ducted Fan Acoustic Radiation Including the Effects of Non-Uniform Mean Flow and Acoustic Treatment," AIAA Paper 93-4424, Oct. 1993.

[3]Eversman, W., "Aft Fan Duct Acoustic Radiation," CEAS/AIAA Paper 95-155, June 1995.

[4]Philbrick, D. A., and Topol, D. A., "Development of a Fan Noise Design System, Part 1: System Design and Source Modeling," AIAA Paper 93-4415, Oct. 1993.

[5]Topol, D. A., "Development of a Fan Noise Design System, Part 2: Far-Field Radiation and System Evaluation," AIAA Paper 93-4416, Oct. 1993.

[6]Heidelberg, L. J., Hall, D. G., Bridges, J. E., and Nallasamy, M., "A Unique Ducted Fan Test Bed for Active Noise Control and Aeroacoustics Research," NASA TM-107213, May 1996; also AIAA Paper 96-1740, May 1996.

[7]Sutliff, D. L., Nallasamy, M., Heidelberg, L. J., and Elliott, D. M., "Baseline Acoustic Levels of the NASA Active Noise Control Fan Rig," NASA Paper TM-107214, May 1996; also AIAA Paper 96-1745, May 1996.

[8]Tyler, J. M., and Sofrin, T. G., "Axial Flow Compressor Noise Studies," *SAE Transactions*, Vol. 70, 1962, pp. 309–332.

[9]Cumpsty, N. A., "A Critical Review of Turbomachinery Noise," *Journal of Fluids Engineering*, Vol. 99, June 1977, pp. 278–293.

[10]Rice, E. J., Heidmann, M. F., and Sofrin, T. G., "Modal Propagation Angles in a Cylindrical Duct with Flow and Their Relation to Sound Radiation," NASA TM-79030, Jan. 1979.

[11]Homicz, G. F., and Lordi, J. A., "A Note on the Radiative Directivity Patterns of Duct Acoustic Modes," *Journal of Sound and Vibration*, Vol. 41, No. 3, 1975, pp. 283–290.

[12]Savkar, S. D., "Radiation of Cylindrical Duct Acoustic Modes with Flow Mismatch," *Journal of Sound and Vibration*, Vol. 42, No. 3, 1975, pp. 363–386.

[13]Rice, E., and Saule, A., "Far-Field Radiation of Aft Turbofan Noise," NASA TM 81506, April 1980.

[14]Rice, E. J., "Multimodal Far-Field Acoustic pattern Using Mode Cutoff Ratio," *AIAA Journal*, Vol. 16, No. 9, 1978, pp. 906–911.

[15]Rice, E. J., "Optimum Wall Impedance for Spinning Modes—A Correlation with Mode Cutoff Ratio," *Journal of Aircraft*, Vol. 16, No. 5, 1979, pp. 336–343.